

REPORT

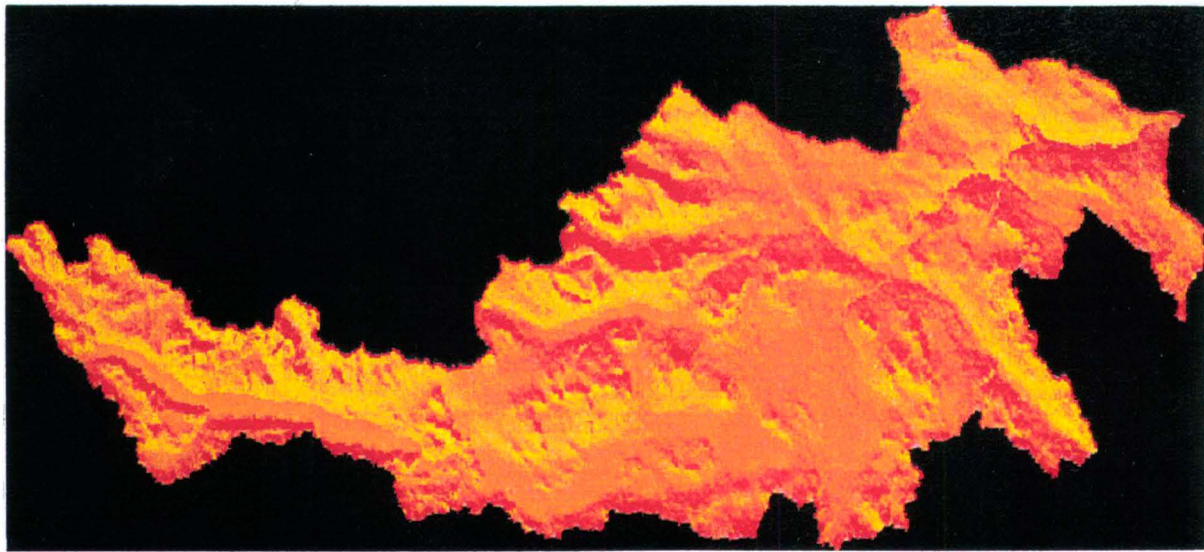
1 1998



Norwegian
Water Resources and
Energy Directorate

Robin Kirschbaum

Development of a gridded degree-day snow accumulation/ablation model with spatio-temporally varying melting factor

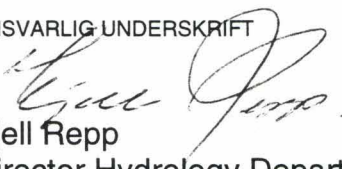


TITTEL Development of a gridded degree-day snow accumulation/ablation model with spatio-temporally varying melt factor	REPORT no 1, 1998
SAKSBEHANDLER Robin Kirschbaum	DATO 23. september 1998
OPPDRAKTSGIVER Dept. of Hydrology, Section Waterbalance	RAPPORTEN ER OPPLAG 35

ABSTRACT

A gridded snow accumulation/ablation model (GSM) is developed. The model is a degree-day approach which spatially distribute the melt factor based on spatial variability of the net solar radiation derived from a digital elevation model (DEM). The temporal variability of the melt factor is modelled as a sinusoid with a minimum in January and a maximum in June. The model provides results which are in better accordance with snow course observations than simulations from the HBV model, and comparison of GSM predicted snow areal extent with satellite images for the melting season is in excellent spatial agreement.

EMNEORD
Snow, gridded model, ablation, accumulation

ANSVARLIG UNDERSKRIFT

 Kjell Repp
 Director Hydrology Department

**Development of a gridded
degree-day snow accumulation/ablation model with
spatio-temporally varying melt factor**

Robin Kirschbaum
NVE and University of Washington
March, 1998

Table of Contents

1	Introduction.....	1
2	Model description	3
2.1	Application over a grid	3
2.2	Spatio-temporal variability in the melt factor	3
2.3	Required input files	4
3	Model implementation	4
3.1	Basin Description.....	4
3.2	Data and parameter specification	7
3.2.1	Digital elevation model	7
3.2.2	Net radiation image.....	9
3.2.3	Meteorological data.....	11
3.2.4	Parameter values	12
4	Results.....	12
4.1	Accumulation.....	13
4.1.1	Subbasin scale	13
4.1.2	Basin scale.....	15
4.2	Ablation.....	17
5	Conclusions.....	20
6	References	21
7	Appendix	23
7.1	Global parameter file.....	23
7.2	Station information file	24
7.3	Print information file.....	24
7.4	DEM and header information	25
7.5	NRI.....	25

1 Introduction

Approximately half of the total land area within Norway lies above the tree line. Precipitation within these alpine regions falls primarily as snow and is stored in deep snow packs over the winter. The amount of water stored in the snow packs and their areal extent strongly influence the timing and magnitude of runoff in the spring. The ability to predict the spatial extent, volume of water storage and melt timing is of critical importance to operational flood forecasting and efficient management of commercial hydropower resources.

Models for predicting snowmelt typically incorporate either an energy balance or temperature-index method. The energy balance approach derives from the principle of conservation of energy. Energy available for melt (Q_m) is computed (Gray and Prowse, 1993):

$$Q_m = Q_n + Q_h + Q_e + Q_g + Q_a - \Delta U/\Delta t \quad [1]$$

where Q_n is the net radiation, Q_h is sensible energy, Q_e is latent energy, Q_g is ground heat, Q_a is advective energy and $\Delta U/\Delta t$ is rate of change of internal energy in the control volume per unit surface area per unit time. This approach offers the ability to explicitly represent the variables which drive snowmelt and, depending on the quality of the input data, simulate the melt process with a high degree of skill.

Because of the intensive data demands of the energy balance approach, degree-day models are often used as an alternative. The degree-day method uses a temperature threshold to indicate the onset of melting. Melt is commonly expressed (Gray and Prowse, 1993):

$$M = Cx * (T - Ts) \quad [2]$$

where M is melt (mm/day), Cx is the melt factor (mm/ 0C /day), T is the average daily air temperature (0C) and Ts is the temperature threshold above which melt occurs (0C). In many applications, the degree-day model produces melt predictions which are comparable to those given by energy balance models. In addition, degree-day models are much simpler to implement because mean daily temperature is relatively easy to measure and forecast (Gray and Prowse, 1993).

Although the melt factor can give a reasonable estimate of an average energy flux, the degree-day approach cannot adequately represent the physics involved when other melt factors such as solar radiation and topography largely control the melt process (Kustas et al., 1994). In order to improve the physics of the degree-day model, Martinec (1989) used a restricted degree-day radiation balance approach to model snowmelt:

$$M = a_r T_d + m_q R_n \quad [3]$$

where, a_r is the restricted degree-day factor, m_q converts energy flux density to melt depth ($\text{cm/day}/(\text{W/m}^2)$) and R_n is the net radiation (W/m^2). With this method, net radiation is disaggregated from the bulk melt factor and allowed to vary independently. He found that the combined degree-day/radiation model improved the degree-day approach and performed comparably with a full energy balance model. Kustas et al. (1994) also used the above approach and found that the restricted degree-day method is more physically representative of the processes it is intended to represent.

A key issue not addressed in the above studies is how to incorporate topographic variability in the calculation of net radiation. Complex topography can have considerable influence on the radiation balance at any point by obstruction, reflection and emission of radiation from surrounding terrain (Dozier, 1980; Dubayah, 1994; Male and Granger, 1981). Kustas et al. underscore the significance of these topographic effects in alpine basins where the larger snow covered areas have slopes ranging between 10^0 and 30^0 . Dubayah (1994) found that the effects of complex topography on net solar radiation in the Rio Grande River Basin in June, 1990 dominated the influence of other factors, such as reflectance. Although computation of the intermediate topographic parameters can be time consuming, Geographic Information Systems (GIS) running on fast, new generation workstations greatly improve the efficiency of this task (Dubayah and Rich, 1995).

This study uses net radiation information to improve the physical basis of the degree-day method. The model proposed is a gridded snow accumulation/ablation model (GSM) which represents spatio-temporal variability in the melt factor. A normalized topographic solar radiation scene (i.e. - for a cloudless, mid-summer day) is used to describe spatial variability in the melt factor. The net radiation image (NRI) is calculated from a digital elevation model using Image Processing Workbench (IPW) software (Frew, 1990), which accounts for modulation of solar radiation at each pixel by surrounding terrain. Temporal variability in the melt factor is sinusoidal with a maximum in June and minimum in January.

The remainder of this paper describes the application of GSM to an unvegetated, alpine region of the Glomma catchment in southern Norway. The model was implemented with a daily time step at 1-km spatial resolution for the period 1980 - 1996. GSM simulations of snow water equivalent (SWE) and snow areal extent (SAE) were compared with simulations from a lumped degree-day model (Lundquist, 1998) and with snow course data and satellite-derived images of snow areal extent (snowmap). GSM predicted SWE was in better agreement with the snow course records than the lumped model, cutting HBV prediction error by 80% in several seasons and by 30% averaged over the simulation period. Comparison of GSM simulated SAE with a snowmap depicting the late 1995 melt season showed excellent spatial agreement.

2 Model description

GSM is a gridded degree-day model with similar parameterizations as the Nordic HBV submodel of Sælthun (1995). Key features which distinguish GSM from HBV and other lumped degree-day models include implementation over a grid and representation of spatio-temporal variability in the melt factor.

2.1 Application over a grid

The benefits of using a distributed model verses a lumped model are mainly that it allows for more physically based input data and gives the opportunity to evaluate model output using available observations, such as field measurements taken at points within a region and satellite images of snow cover. Furthermore, it is easier to use a distributed model because specification of important physical information such as topography and radiation can reduce the need for heavy manual calibration of conceptual parameters. In this application, topography and net radiation were the distributed inputs and simulated SWE and SAE were the distributed outputs.

2.2 Spatio-temporal variability in the melt factor

GSM uses a unique method of spatially distributing the melt factor over the grid. The method is based on a normalized net radiation image (NRI) which is calculated using a topographic radiation algorithm to account for obstruction, reflection and emission of

radiation on each pixel from surrounding terrain. Section 3.2.2 discusses how the NRI was prepared.

Monthly variability in the melt factor is sinusoidal (Gray and Prowse, 1993) with maximum and minimum values in June and January, respectively. The use of a sinusoidal function to distribute the melt factor is subjective. Field data are necessary to evaluate the true seasonality in the melt factor for a given region.

2.3 Required input files

GSM requires 5 major input files, including a global parameter file, station information file, print information file, digital elevation model (DEM) with header information and net radiation image (NRI). A sample of each input file is provided in the Appendix.

3 Model implementation

The model was implemented at 1-km resolution for Vinstra in Southern Norway for the period 1980 - 1996 using a daily time step. In this section, a physical description of Vinstra as well as discussion of data and parameters used to drive the model are provided.

3.1 Basin Description

Vinstra is a small subcatchment (approximately 1,600 km²) in the Oppland region of the Glomma basin in Norway. Figure 1 shows the location of Vinstra and Glomma within southern Norway. The basin contains six major lakes, including Bygdin, Heimdalsvatn, Oeyangen, Olstappen, Kaldfjord and Vinsteren. The catchments of these lakes were used to evaluate model performance at the subbasin scale. Figure 2 shows the locations and areas of each subbasin.

Vinstra is an unvegetated, alpine catchment with mean elevation of approximately 1,100 m. Topographic variability is significant, with the Jotunheimen Mountains forming the northern boundary and the Olstappen Valley covering much of the eastern portion of the basin. Mean annual precipitation ranges approximately between 400 and 2,500 mm/yr, with highest precipitation occurring in the mountainous north and lowest in the eastern valley.

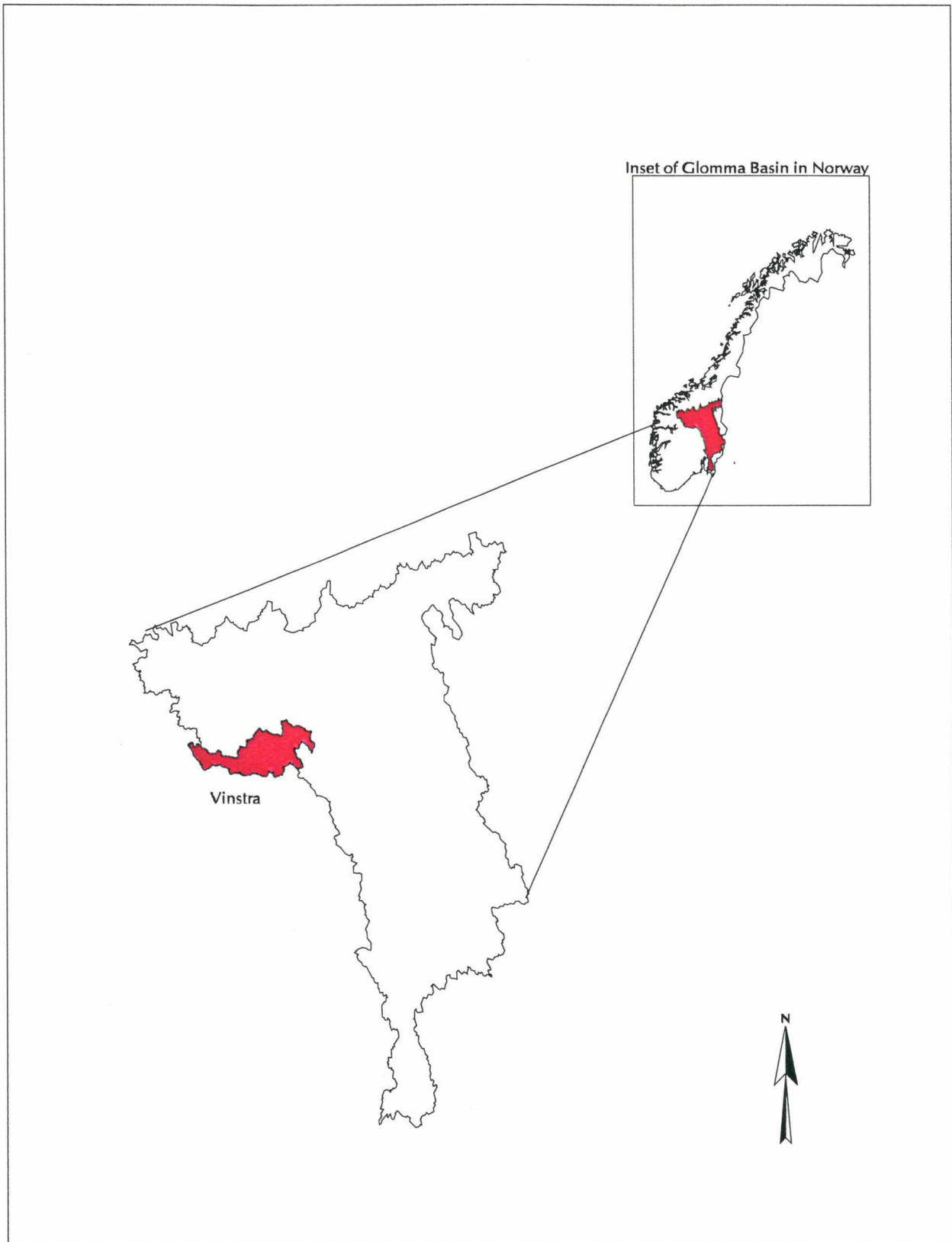


Figure 1. Location of Vinstra within the Glomma Basin in southern Norway

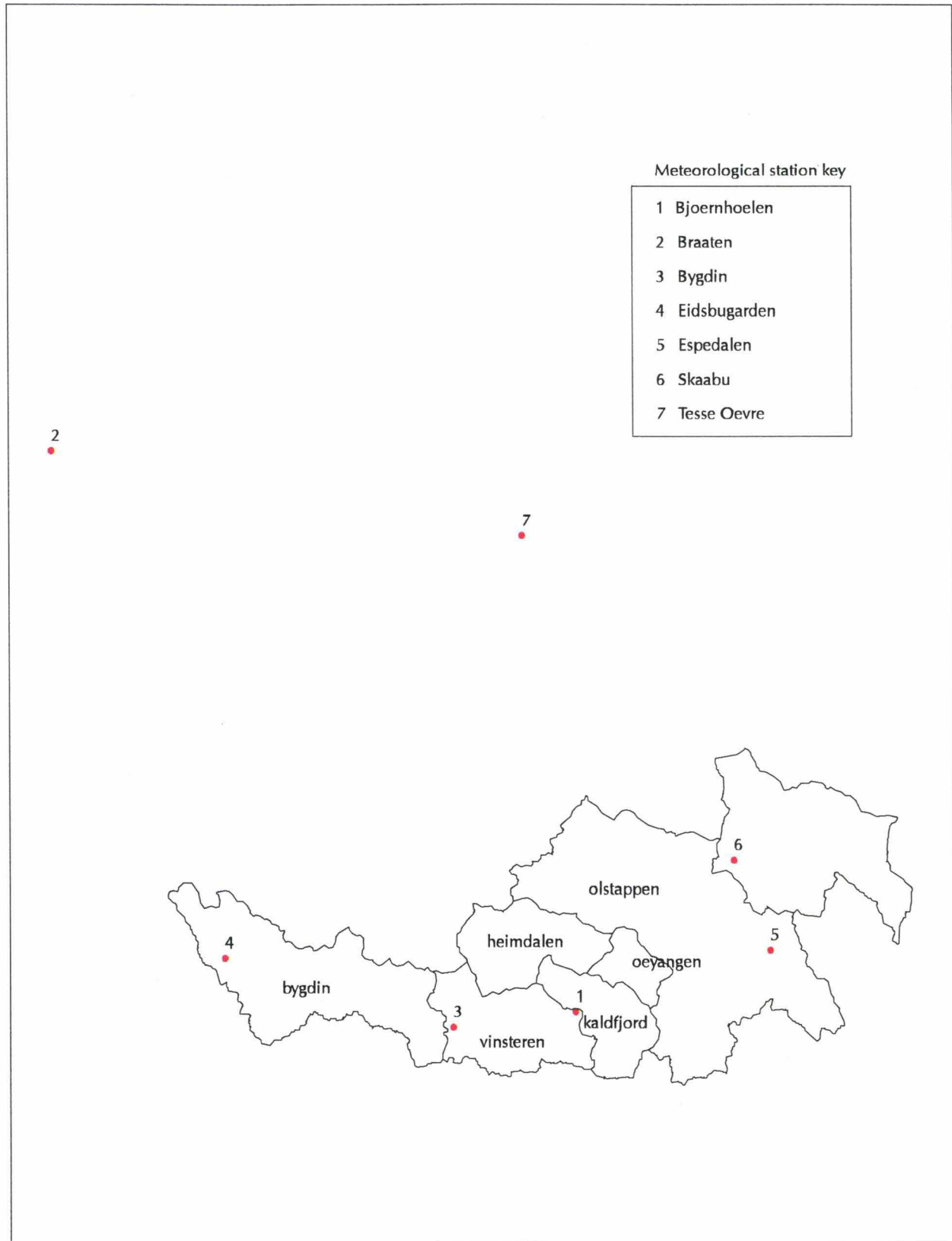


Figure 2. Location of meteorological stations and subbasin delineation.

3.2 Data and parameter specification

This section describes the driving data, which include a digital elevation model, net radiation image and daily precipitation and maximum and minimum air temperature. Description of model parameters and values used in this application is provided.

3.2.1 Digital elevation model

A DEM provided by the Norwegian Mapping Agency with 100-m resolution and an accuracy of approximately 10 m was used (Figure 3). The DEM was used to prepare the NRI (Section 2.2) and to lapse temperature and precipitation from the stations to the mean grid cell elevations (Section 3.2.3). In the first application, the raw DEM was used. Dubayah and Rich (1995) warn about the dangers of significant errors propagating from low quality DEMs to calculation of net radiation. It is believed that the DEM was of sufficient resolution and quality for this purpose, since the NRI was ultimately aggregated to 1-km resolution. In the second application, the DEM was aggregated by the mean pixel value to 1-km resolution.

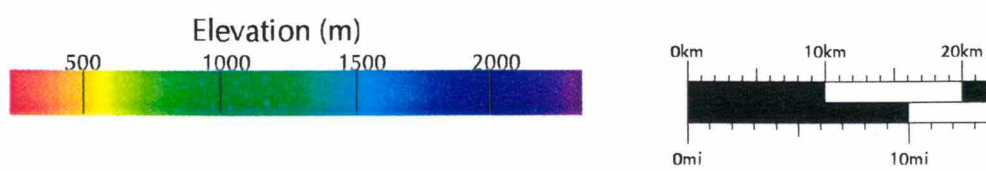
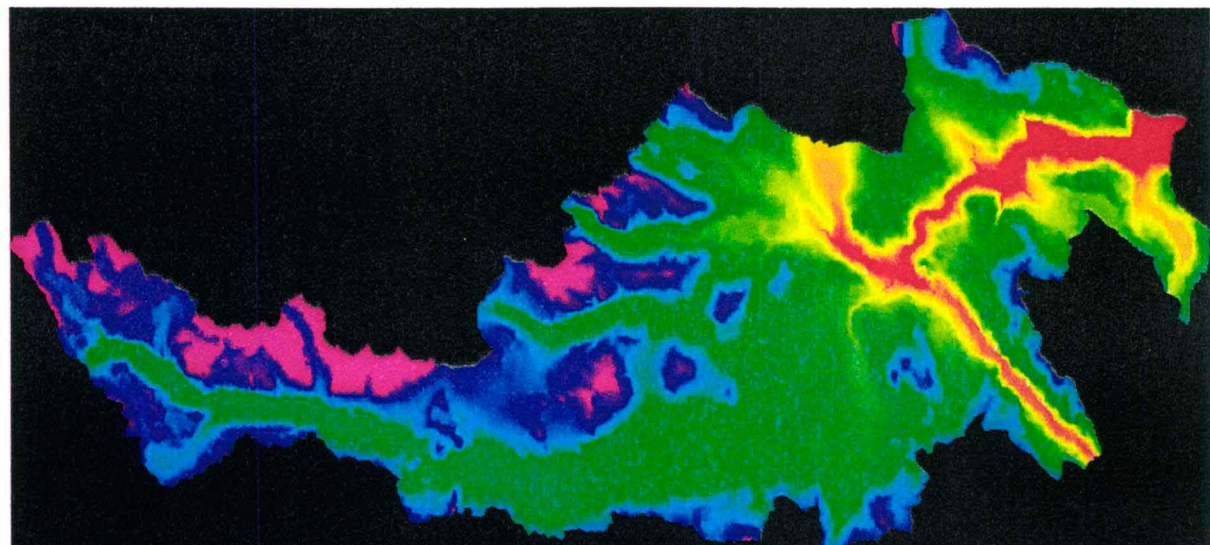


Figure 3. 100-m resolution digital elevation model (DEM).

3.2.2 Net radiation image

The NRI was calculated with the DEM as input and normalized by the mean value. A mid-June solar position with clear sky conditions and a global albedo of 0.7 were assumed. The assumption of a mid-June solar position was arbitrary and has no effect on the resulting normalized NRI when coupled with the assumptions of clear sky and global albedo. The latter two assumptions were made in order to capture the static variability in net radiation, as the distribution of cloud cover and albedo can change drastically over relatively short time increments. See Appendix 7.5 for the IPW commands used to prepare the NRI.

Figure 4 shows the NRI, with yellow indicating high values of net radiation and red indicating low values. A sharp band of red pixels (low net radiation) appears along the northeastern boundary of the basin. This is likely an artifact of improper masking of the basin during preparation and should be corrected.

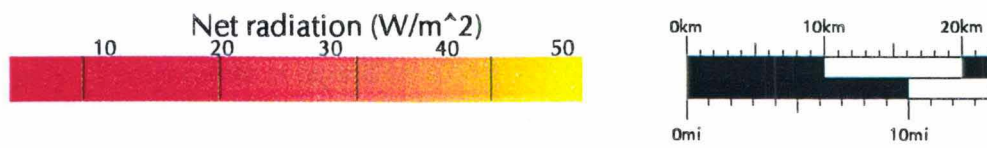
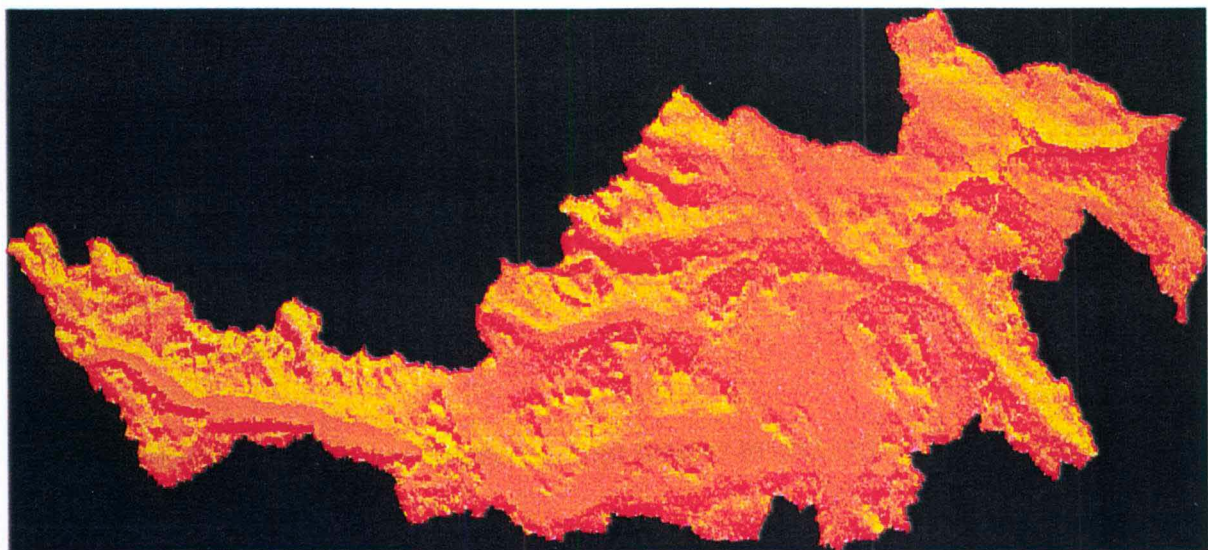


Figure 4. Net radiation image (NRI).

3.2.3 Meteorological data

Daily precipitation and maximum and minimum temperature from six stations for January, 1980 to December, 1996 were provided by Lundquist (1998). See Figure 2 for station locations. Table 1 lists the stations with their precipitation and snow correction factors (Pcorr and Scorr) used to correct for gauge catch deficiencies. Also defined for each station are switches, prcp and temp, used to indicate whether the station was used to provide precipitation and/or temperature data, respectively. In both cases, a switch value of 1 indicates the station is being used.

Table 1 Meteorological station names, precipitation correction factors, snow guage correction factors and switch values indicating whether or not the station was used to provide precipitation and/or temperature data.

	Pcorr	Scorr	prcp	temp
Bjoernhoelen	1.0	1.05	1	0
Braaten	1.2	1.05	1	1
Bygdin	1.3	1.3	1	1
Eidsbugarden	1.0	1.0	1	0
Espedalen	1.05	1.25	1	0
Skaabu	1.05	1.0	1	1
Tesse Oevre	1.0	1.0	1	1

* Figure 2 shows station locations.

Meteorological data are distributed from stations to grid cells according to:

1. distance from station to grid cell
2. elevation gradient between station and grid cell

A least-distance squared method using two nearest neighbors is used to distribute the data horizontally. Temperature is lapsed by a constant rate of $-0.6^{\circ}\text{C}/100 \text{ m}$ gradient in elevation between station and grid cell and precipitation by 10%/km.

The sparsity of the meteorological stations is presumed to be the greatest source of error in this study. Although it would be theoretically interesting to use a higher resolution, better quality DEM to prepare the NRI, it is believed that the error in interpolating such a

sparse set of meteorological data would mask the benefits of increasing the resolution of any other inputs.

3.2.4 Parameter values

Important parameters include a maximum and minimum melt factor, Cx_{max} and Cx_{min} , respectively, a rain/snow temperature threshold, T_x and a melting threshold temperature, T_s . All parameters were specified globally in this application. In Lundquist (1998), model parameters were optimized separately for the six subcatchments. Table 2 shows a comparison of parameter values used in this study along with the range of values used by Lundquist.

Table 2 Parameter values used in this study and in Lundquist (1998). A "*" indicates high model sensitivity to that parameter. "N/A" means the parameter was not used.

Parameter name	Symbol	Value used in this application	Range of values used by Lundquist (1998)
Rain/snow temperature threshold	T_x^*	1.0	1.0 - 1.1
Melt temperature threshold	T_s^*	0.3	0.0 - 1.5
Maximum melt factor	Cx_{max}	4.0	N/A
Minimum melt factor	Cx_{min}	1.0	N/A
Melt factor	Cx	N/A	3 - 4

4 Results

This section presents results from daily simulations of SWE and SAE for Vinstra made with GSM. Snow course data for March and late April provided by Lundquist served as SWE observations in the late accumulation period. GSM predicted SWE are compared with simulations made using the HBV (Lundquist, 1998). Snowmaps processed by the Norwegian Water Resources and Energy Administration (NVE) from raw satellite data were used to evaluate GSM simulated SAE during the 1995 melt period.

4.1 Accumulation

The accumulation period is defined between early September and late April, with maximum accumulated SWE assumed to occur in late April. GSM simulations of maximum SWE were compared with distributed snow course observations taken in late April of each year and with HBV simulations at the subbasin and basin scales.

4.1.1 Subbasin scale

Observed SWE at the subbasin scale were derived by distributing snow course observations from point locations to the subbasins using subjective algorithms (Lundquist, 1998). Figure 5 shows percent error calculated for GSM and HBV simulations for each of the six subbasins, which is expressed:

$$\% \text{ error} = \text{ABS}(\text{observed} - \text{simulated}) / \text{observed} * 100 \quad [4]$$

GSM shows significant improvement over HBV in simulating maximum accumulation in the larger subbasins, including Bygdin, Vinsteren and Olstappen. Highest improvement was realized in Bygdin, where GSM errors averaged over the simulation period were 40% lower than HBV. Better GSM simulation of maximum SWE is likely the result of using a DEM to lapse meteorological data to the grid cell elevation. The two models perform relatively comparably in Oeyangen. GSM results have a slightly higher error than HBV in the remaining two subcatchments, Heimdalsvatn and Kaldefjord. GSM overpredicted maximum SWE in these regions by 45 and 35%, respectively, averaged over the simulation period. Poor GSM performance in these subcatchments is attributed to the data and/or parameters Pcorr and Scorr (Table 3.1) assigned to the meteorological station Bjoernhoelen, which contributed most of the data to these regions.

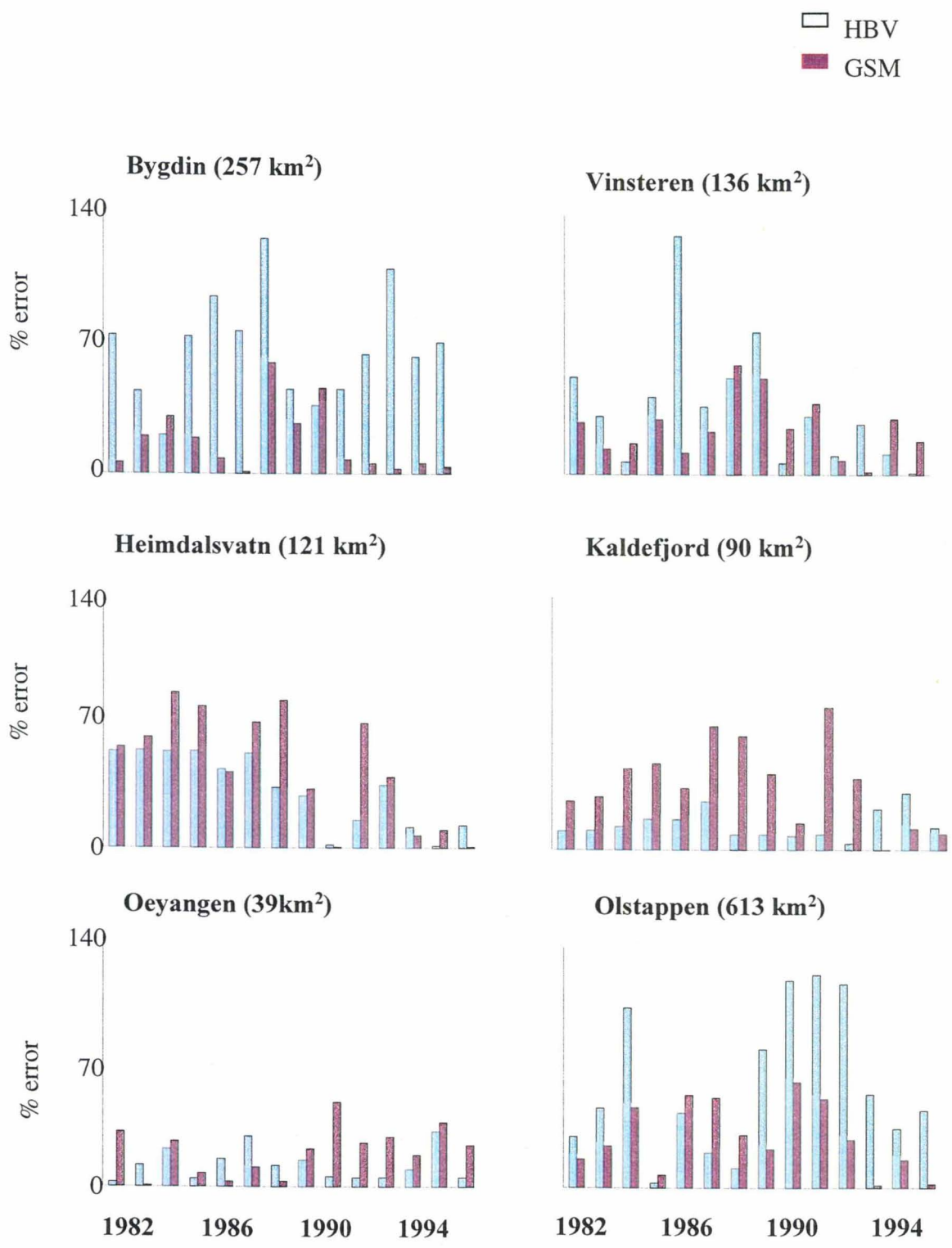


Figure 5. Percent error in GSM and HBV simulated maximum accumulated SWE at the subcatchment scale.

4.1.2 Basin scale

Snow course estimates of SWE for each of the subbasins were areally averaged to derive observed SWE for the entire basin. These were the basis for evaluating and comparing GSM and HBV basin-averaged simulated SWE. Figure 6 shows observed, HBV simulated and GSM simulated SWE. For most simulation years, both HBV and GSM overpredict maximum accumulated SWE. GSM predictions are generally significantly closer to the observed values than HBV. Figure 7 better illustrates the comparative model errors (Eq. 4). Averaged over the simulation period, GSM has a mean error of approximately 16% and HBV approximately 23%.

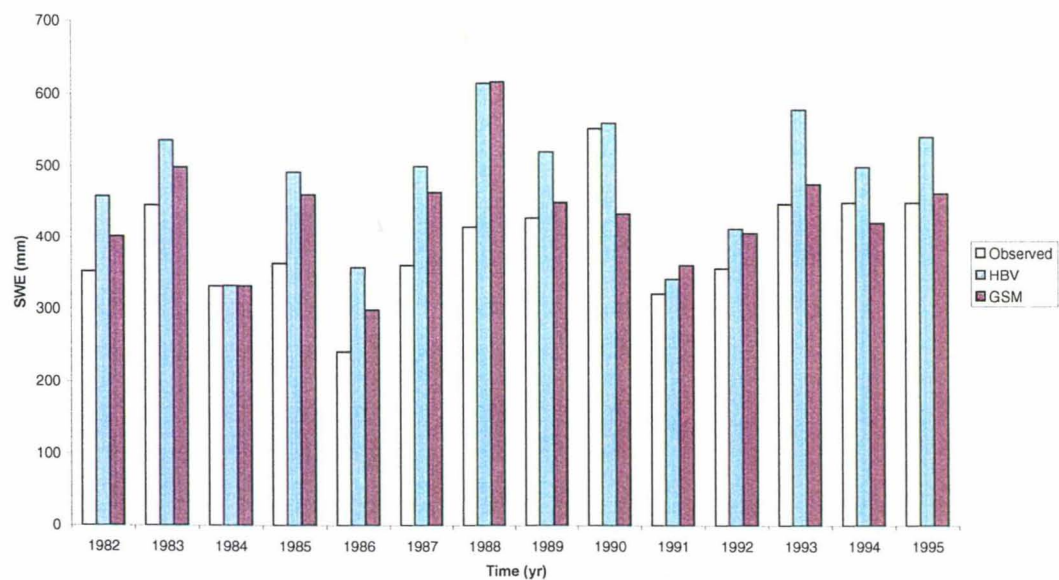


Figure 6. Observed, GSM and HBV simulated maximum accumulated SWE at the catchment scale.

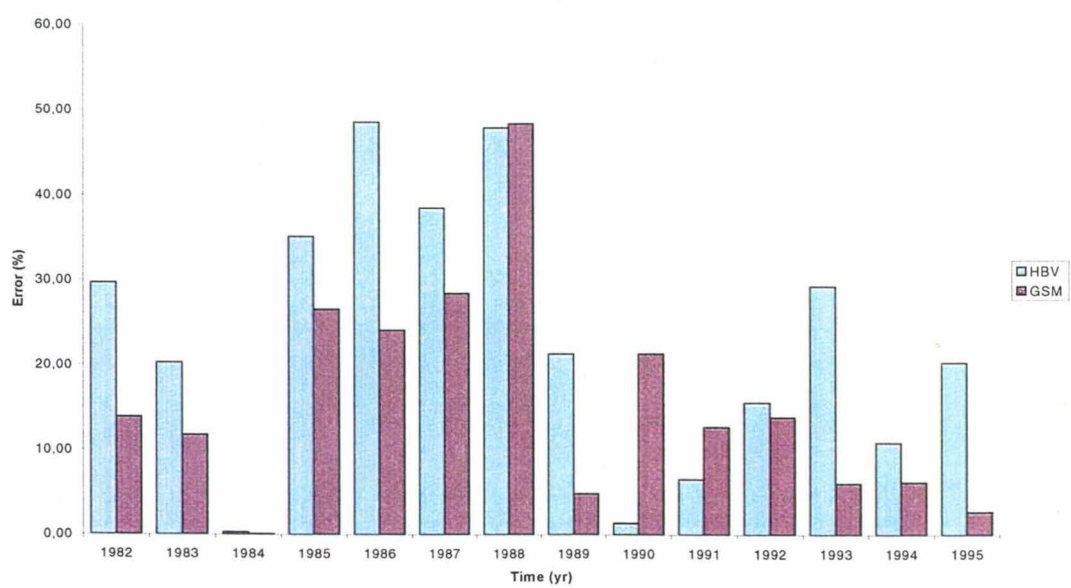


Figure 7. Percent error in GSM and HBV simulated maximum accumulated SWE at the catchment scale.

4.2 Ablation

Snow maps derived from satellite reflectance images for May 22 and June 13 were used to evaluate GSM simulated snow areal extent (SAE) during the 1995 melting season.

Predicted SAE is evaluated as the total area containing grid cells which have simulated SWE $> \text{SWE}_{\text{threshold}}$, where $\text{SWE}_{\text{threshold}}$ was taken as 5 mm in this application. Observed SAE is evaluated as the total area containing grid cells with snow coverage $> 0\%$. Figures 8 and 9 depict the a) digital elevation model, b) snowmap, c) simulated SWE with spatio/temporal variability in Cx, d) simulated SWE with only temporal variability in Cx, e) computed errors in the timing of melt for the simulation with spatio/temporal variability in Cx and f) computed errors in the timing of melt for the simulation with only temporal variability in Cx. In plates e) and f), a pink-colored grid cell indicates that the timing of snow melt for that grid cell was late, i.e. - the snowmap at the location of that grid cell shows bare ground while simulated SWE is greater than 5 mm. Conversely, a blue-colored grid cell indicates early snow melt and a green-colored grid cell indicates agreement in timing of melt between the simulation and the snowmap.

On May 22, 1995 (Figure 8), plates e) and f) are identical. Later in the season, as depicted in the June 13 image (Figure 9), the simulation made with the spatially varying melt factor has fewer late melting grid cells than the simulation made with a non-spatially distributed melt factor. Thus, the spatially distributed melt factor has no apparent effect early in the season, but has a significant effect in improving predicted SAE as melting progresses. It should be noted that this analysis is highly sensitive to the threshold simulated and observed SWE (5mm) and SAE (0%) values used. Furthermore, the results are inconclusive due to an insufficient number of available high quality snowmaps.

Note that in plate e) of Figure 9 several grid cells at the eastern edge of the basin show late melt. This appears to be a result of the artificially low NRI values at the eastern basin boundary which was attributed to improper masking during the preparation of the NRI (Section 3.2.2).

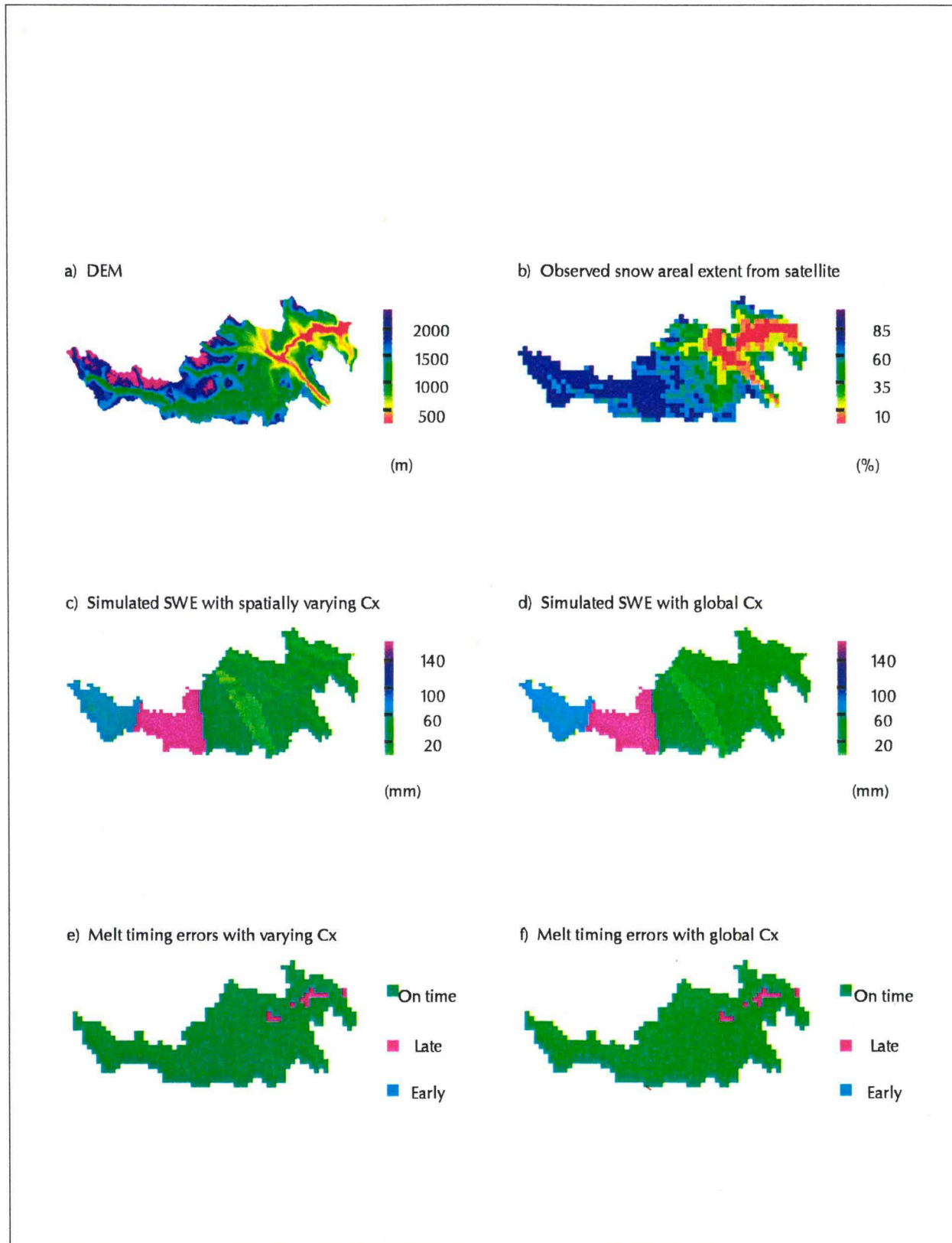


Figure 8. Results from 1995 melt season, May 22.

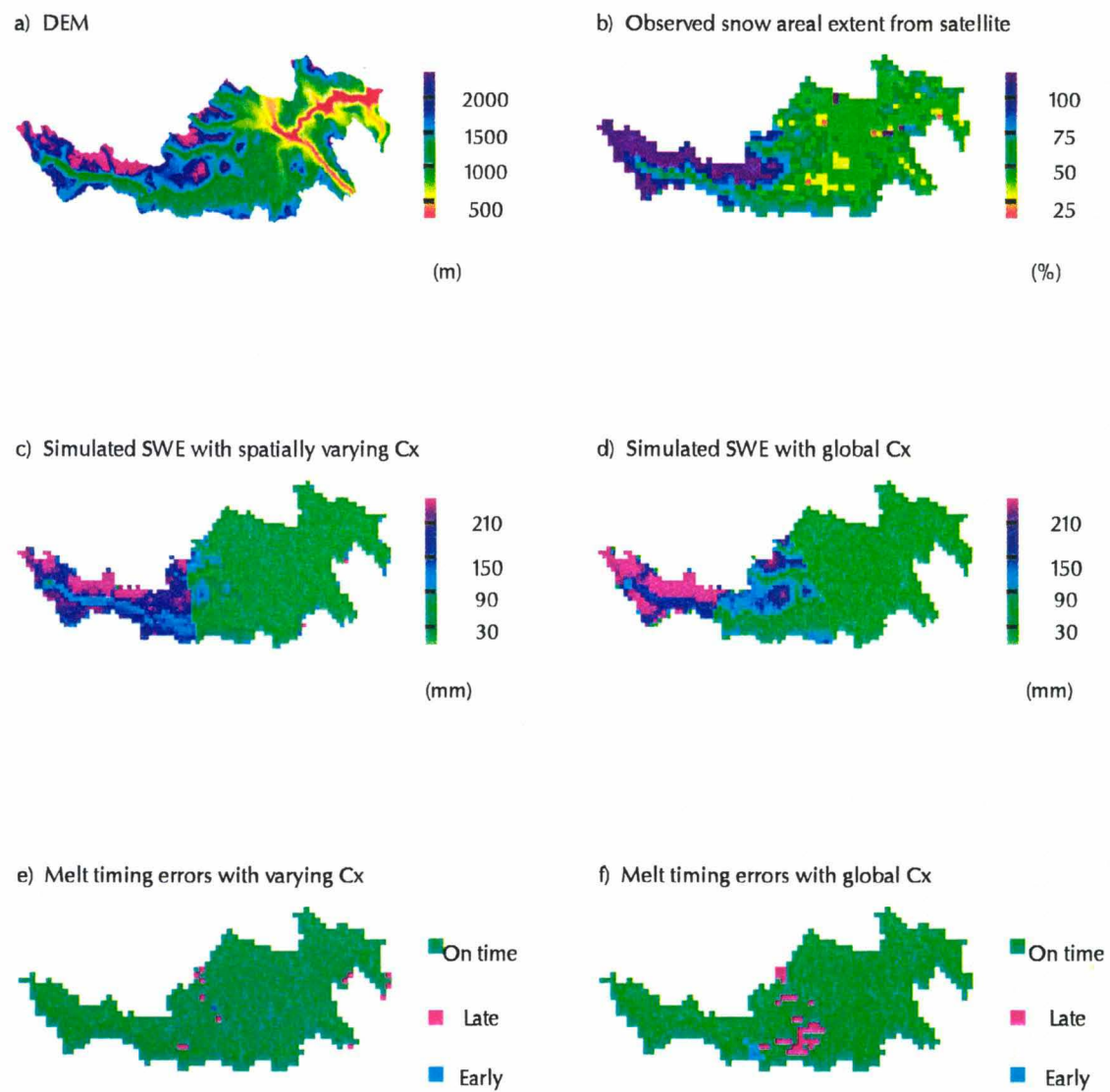


Figure 9. Results from 1995 melt season, June 13.

5 Conclusions

A gridded snow model, GSM, has been developed. GSM uses a degree-day approach with spatial and temporal variability in one of the most important model parameters, the melt factor. A unique method was used to represent spatial variability in the melt factor. The method is based on a normalized topographic net solar radiation image (NRI) derived using algorithms which account for obstruction, reflection and emission of solar radiation on each pixel from surrounding terrain. Temporal variability is sinusoidal with a minimum in January and maximum in June.

The model was tested in the Vinstra catchment for the period 1980 - 1996. Results from daily simulations were compared with snow course observations of maximum SWE in the accumulation period and satellite derived snowmaps in the melting period. Model performance was also compared with HBV simulations. GSM greatly improved prediction of maximum SWE in the three largest subbasins and for the basin averaged SWE, while HBV had slightly lower simulation errors for the three smallest subbasins. The improvement at the basin scale may be attributed to the use of a DEM to distribute the meteorological data.

Comparison of observed and predicted SAE for June 13, 1995 indicates that the spatially distributed melt factor can significantly improve model performance during the ablation period. Several more high quality snowmaps are needed, however, to better analyze the effectiveness of the spatially varying melt factor.

6 References

- Blöschl, G., Gutknecht, D. and Kirnbauer, R., Distributed snowmelt simulations in an alpine catchment: 2. Parameter study and model predictions, W.R.R., Vol. 27, No. 12, pp. 3181-3188, Dec., 1991.
- Blöschl, G., Kirnbauer, R. and Gutknecht, D., Distributed snowmelt simulations in an alpine catchment: 1. Model evaluation on the basis of snow cover patterns, W.R.R., Vol. 27, No. 12 3171-3179, Dec., 1991.
- Dozier, J., A clear-sky spectral solar radiation model for snow-covered mountainous terrain, W.R.R., Vol. 16, No. 4, 709-718, August, 1980.
- Dozier, J. and Outcalt, S. I., an Approach toward energy balance simulation over rugged terrain, Geographical Analysis, Vol. 11, No. 1, January, 1979.
- Dubayah, R., Estimating net solar radiation using landsat thematic mapper and digital Elevation Data, W.R.R., Col. 28, No. 9, 2469-2484, Sep. 1992.
- Dubayah, R.C., Modeling a solar radiation topoclimatology for the Rio Grande River Basin, J. of Veg. Science, 5: 627-640, 1994.
- Dubayah, R. and Rich, P.M., Topographic solar radiation models for GIS, Int. J. Geographical Information Systems, Vol. 9, No. 4, 405-419, 1995.
- Elder, K., Dozier, J. and Michaelsen, J., Snow accumulation and distribution in an alpine watershed, W.R.R., Vol. 27, No. 7, 1541-1552, July, 1991.
- Frew , Jr., J.E., 1990. The Image Processing Workbench. Ph.D. Dissertation, University of California, Santa Barbara, CA.
- Gray, D. M. and Prowse, T. D., Handbook of Hydrology, Chapter 7, McGraw-Hill, Inc., New York, Editor in Chief David R. Maidment, 1993.
- Kustas, W.P. and Rango, A., A simple energy budget algorithm for the snowmelt runoff model, W.R.R., Vol. 30, No. 5, 1515-1527, May, 1994.
- Lundquist, D., Advisor at Glommens og Laagens Bruksseierforening, Oslo, Norway, conversation, October - March, 1998.
- Male, D. H. and Granger, R. J., Snow surface energy exchange, W.R.R., Vol. 17, No. 3, 609-627, Jun , 1981.
- Marks, D., J. Dozier, Climate and enrgy exchange at the snow surface in the alpine region of the Sierra Nevada, 2, snow cover energy balance, W.R.R., Vol 28, 3043-3054, 1992.

Martinec, J., Hour-to-hour snowmelt rates and lysimeter outflow during an entire ablation period, in Snow Cover and Glacier Variations, Proceedings of the Baltimore Symposium, Maryland, May, 1989, edited by A. Rango, IAHS Publ., 183, 19-28, 1989.

Sælthun, N.R., "Nordic" HBV Model, Norwegian Water Resources and Energy Administration, February 26, 1995.

7 Appendix

The following provides samples and/or descriptions of all input files required to run GSM, including a global parameter file, station information file, print information file, digital elevation model (DEM) and header information and normalized net radiation image (NNRI). A number and hash mark ("#") appear before each line of input in most of the samples for the sake of reference, but should not appear in the actual input files.

7.1 Global parameter file

```
#1      1000
#2      135719
#3      6848215
#4      1980 1 1 1996 12 1
#5      1994 9 1
#6      24
#7      1.5
#8      1.5
#9      6.5
#10     1.0
#11     0.01
#12     0.1

#1      Resolution of model grid mesh in meters. Thus, in the example, the length of one side
       of a single grid cell is 1000 meters.
#2      The y-coordinate of the center of the upper-left-hand grid cell in UTM 33.
#3      The x-coordinate of the center of the upper-left-hand grid cell in UTM 33.
#4      Begin year, month, day and end year, month, day of input daily station meteorological
       data (raw data).
#5      Start year, month, day of model run.
#6      Time step for model calculation in hours (this should not be changed in this version of
       the model).
#7      Tx - Threshold temperature below which precipitation occurs as snow (in degC).
#8      Ts - Threshold temperature used in computing the number of degree-days.
#9      Cxmax - Maximum monthly melt factor assigned to occur in June.
#10     Cxmin - Minimum monthly melt factor assigned to occur in January.
#11     Cfr - Refreezing efficiency
#12     Fmax - Maximum relative free water before runoff.
```

7.2 Station information file

#1	file_name	E	N	h.a.s.l.	prcp	temp	pcorr
	scorr						
#2	/usr/home/rwk/sta1	183795 1.25	6817053	1025	1	0	1.05
#3	/usr/home/rwk/sta2	183900 1.01	6817123	700	1	1	1.25

#1 is a header line. The program is expecting this line. The first column in the following lines provides the exact path name for the meteorological data file. The second, third and fourth provide the Easting, Northing (in UTM 33) and hight above sea level (in meters), respectively. The fourth and fifth columns indicate whether or not the station is to be used to provide precipitation and/or temperature data (1 indicates yes, 0 indicates no), respectively. The sixth and seventh columns are precipitation and snow gauge correction factors, respectively.

7.3 Print information file

This file designates days for which spatial images of model simulated snow water equivalent (SWE) will be printed. The images will be output as a single string of binary characters with (number of rows x number of columns) bytes. In this example, only one spatial image of SWE will be output for March 29, 1995.

```
#1    1995  29    3
```

The unix command: rawtopgm <ncols> <nrows> sim.3_29_1995 | xv - can be used to view the output. The file could also be imported into Arc/Info as a ".bil" file with an appropriate Arc/Info ascii header.

Warning: The data within the printed images are written as binary characters (values ranging between 0 and 254). Thus, if the range of data written is outside 0 -254, the values will automatically wrap. I.E., An SWE value of 255 will be written as 0, 256 will be written as 1, etc.

7.4 DEM and header information

The DEM is read as a single string of binary characters with (number of rows * number columns) bytes. Each character represents a mean grid cell elevation in meters. Because of the inherent limited range of values for a binary character (0 - 254), the data must be coded in order to fit within this range. For example, if the maximum mean grid cell elevation is 2,500 meters, you might choose to scale all values by a factor of 1/10.

An ascii header file must also be supplied:

```
#1    878  
#2    398  
#3    135669.844  
#4    6848265.0  
#5    100
```

```
#1    Number of columns in DEM.  
#2    Number of rows in DEM.  
#3    Y-coordinate of the upper-left-hand DEM grid cell in UTM 33.  
#4    X-coordinate of the upper-left-hand DEM grid cell in UTM 33.  
#5    Resolution of DEM in meters.
```

Note: The resolution of the DEM is expected to be equal to or finer than the model grid mesh resolution.

7.5 NRI

The NRI is read in the same manner as the DEM. Thus, it must be a single string of binary characters with (number of rows x number of columns) bytes. Following are sample IPW commands used to derive the NRI:

Consider the digital elevation model for the Vinstra catchment represented by 398 rows and 878 columns, named "vinstra.in". Refer to an IPW user's guide (<http://ice.cor.epa.gov/%7Eipw/www/userGuide/cmdIndex.html>) for a complete description of all the arguments used in the following series of commands.

1. Import an ascii DEM into IPW. The DEM must have 0 as the NODATA value. The image must also be stripped of all header information. The command would then be:

```
iimport -l 398 -s 878 vinstra.in > vinstra.ipw
```

2. A geographic header must be appended.

```
mkgeoh -o 217625,6949742 -d 100,100 -u meters -c UTM vinstra.ipw > vinstra.geoh
```

3. Compute a 2-band image containing slope and aspect:

```
gradient -d 100 vinstra.geoh > gradient.out
```

4. Compute a 2-band image containing sky view factor and terraing configuration factor:

```
viewf vinstra.geoh > viewf.out
```

5. Compute a 2-band image containing beam and diffuse radiation:

```
elevrad -z 100 -t 0.2 -w 0.85 -g 0.55 -r 0.155 -s 150.214 -u 0.8168 vinstra.geoh > elevrad.out
```

6. Compute a shaded relief map:

```
shade -u 0.8168 -a 120 gradient.out > shade.out
```

7. Separate all multiband images into single band images:

```
demux -b0 elevrad.out > elevrad.b0
```

```
demux -b1 elevrad.out > elevrad.b1
```

```
demux -b0 gradient.out > gradient.b0
```

```
demux -b0 viewf.out > viewf.b0
```

```
demux -b1 viewf.out > viewf.b1
```

8. Construct an image of albedo (alb). In this application, albedo was considered constant across the grid mesh (0.7) and the image was contructed in Arc/Info, GRID mode by equating all grid cells with a dem value > 0 to 0.7.
9. Construct a 6-band image containing the above images for input into the toporad command:

mux elevrad.bo elevrad.b1 shade.out viewf.bo viewf.b1 alb > toporad.in

10. Compute the net radiation image using the input multi-band image derived in step 9.:

toporad -n toporad.in > toprad.out

This series is published by Norwegian Water Resources and Energy Directorate (NVE)
Address: P.O. Box 5091, Majorstua, N-0301 Oslo NORWAY

PUBLISHED IN THIS SERIES:

Nr 1 Robin Kirschbaum: Development of a gridded degree-day snow accumulation/ablation
model with spatio-temporally varying melting factor (28 s.)



**Norwegian
Water Resources and
Energy Directorate**

Norwegian water resources
and energy directorate
Middelthunsgate 29
Postboks 5091 Majorstua
N- 0301 Oslo NORWAY

Telephone: +47 22 95 95 95
Telefax: +47 22 95 90 00
Internet: www.nve.no